# Deep fault plane geometry inferred from multiplet relative relocation beneath the south flank of Kilauea

J.-L. Got

Université de Savoie, Le Bourget-du-Lac, France

J. Fréchet

Laboratoire de Géophysique Interne et Tectonophysique, Observatoire de Grenoble, Grenoble, France

Fred W. Klein

U.S. Geological Survey, Menlo Park, California

**Abstract.** Dense microearthquake swarms occur in the upper south flank of Kilauea, providing multiplets composed of hundreds of events. The similarity of their waveforms and the quality of the data have been sufficient to provide accurate relative relocations of their hypocenters. A simple and efficient method has been developed which allowed the relative relocation of more than 250 events with an average precision of about 50 m horizontally and 75 m vertically. Relocation of these events greatly improves the definition of the seismic image of the fault that generates them. Indeed, relative relocations define a plane dipping about 6° northward, although corresponding absolute locations are widely dispersed in the swarm. A composite focal mechanism, built from events providing a correct spatial sampling of the multiplet, also gives a well-constrained northward dip of about 5° to the near-horizontal plane. This technique thus collapses the clouds of hypocenters of single-event locations to a plane coinciding with the slip plane revealed by previous focal mechanism studies. We cannot conclude that all south flank earthquakes collapse to a single plane. There may locally be several planes, perhaps with different dips and depths throughout the south flank volume. The 6° northward-dipping plane we found is too steep to represent the overall flexure of the oceanic crust under the load of the island of Hawaii. This plane is probably an important feature that characterizes the basal slip layer below the upper south flank of Kilauea volcano. Differences in seismicity rate and surface deformations between the upper and lower south flank could be related to the geometry of this deep fault plane. The present work illustrates how high precision relative relocations of similar events in dense swarms, combined with the analysis of geodetic measurements, can help to describe deep fault plane geometry. Systematic selection and extensive relative relocation of similar earthquakes could be attempted in other well-instrumented, highly seismic areas to provide reliable basic information, especially useful for understanding of earthquake generation processes.

## Introduction

Kilauea Volcano has many geological features of major interest. Indeed, Kilauea Volcano, built on the southeast flank of Mauna Loa Volcano, exhibits beside the caldera, two large rift zones delimiting the south flank, which slides seaward. Other volcanoes (Piton de la Fournaise, Etna, Mount St. Helens) present more or less similar sliding structures. But only at Kilauea Volcano is there almost continuous seismic and eruptive activity, as well as a high horizontal strain rate, related to this movement.

Tectonics and seismicity of the south flank of Kilauea have been extensively studied [*Swanson et al.*, 1976; *Ando*, 1979; *Wyss et al.*, 1981; *Crosson and Endo*, 1982; *Eissler and Kanamori*, 1987; *Klein et al.*, 1987; *Thurber and Gripp*, 1988; *Wyss and Kovach*, 1988; *Arnadottir et al.*, 1991; *Bryan and Johnson*, 1991; *Bryan*, 1992]. These authors all stress the need for a subhorizontal fault plane

at the base of the volcanic pile on the oceanic crust at a depth of about 9 km to explain the seaward movement of the south flank. This fault plane has been inferred from geodetic measurements [*Swanson et al.*, 1976; *Arnadottir et al.*, 1991], from focal mechanisms, surface wave analysis and tsunami records after the Kalapana (1975, $M_s$ = 7.2) earthquake [*Ando*, 1979] but never directly determined from simple earthquake hypocenter locations. Indeed earthquake locations are distributed in ellipsoidal volumes, whose major axis is roughly vertical, ranging from 5- to 10-km depth [*Klein et al.*, 1987]. This distribution does not define a fault plane [*Arnadottir et al.*, 1991]. *Crosson and Endo* [1982] hypothesize that most of the vertical scatter was due to location errors and supported the idea of a sub-horizontal fault plane. *Klein et al.* [1987] and *Thurber and Gripp* [1988] show hypocentral cross-sections and use the base of the seismic zone to define the decollement plane. The use of microearthquake focal mechanisms leads to numerous partial results, but also different interpretations [*Crosson and Endo*, 1982; *Thurber and Gripp*, 1988; *Bryan and Johnson*, 1991; *Bryan*, 1992]. Added to the

uncertainty of the locations, the statistical significance of the focal mechanisms is difficult to estimate. Studies from *Crosson and Endo* [1981] and *Klein* [1981] show the dependence of the focal solutions on the velocity model.

However, the dense swarms of the northernmost part of the south flank could provide events close to one another, allowing the use of a relative relocation method. Such methods have been used to relocate very similar microearthquakes in central California [*Poupinet et al.*, 1984; *Fréchet*, 1985], Japan [*Ito*, 1985], Swabian Jura [*Scherbaum and Wendler*, 1986], Mount St. Helens [*Frémont and Malone*, 1987] and northern Switzerland [*Deichmann and Garcia-Fernandez*, 1991]. These studies generally used few events and cannot infer deep structures on a large extent from the relocations. In this paper, we will see if the use of an extensive set of data recorded in a highly seismic area is able to provide a sufficient number of very similar earthquakes for us to infer, by simple relative relocation, useful information concerning the deep active structures that generate the seismicity.

## Data Selection

The data are microearthquakes recorded from 1979 to 1983 by the Hawaiian Volcano Observatory (HVO) seismic network, which then was composed of 50 telemetered stations distributed throughout the island of Hawaii (Figure 1). These are frequency-modulated signals recorded on 1-in magnetic tapes, then demodulated and digitized at a rate of hundred samples per second. For this study we use only vertical component seismograms.

These data cover a part of the period of intense seismic activity following the Kalapana earthquake (November 29, 1975; $M_s = 7.2$), and come from one of the most active seismic zones of the south flank of Kilauea Volcano (Figure 1). Most south flank seismic activity occurs as dense microearthquake swarms ($m_l \leq 3.5$). To retain the greatest possible number of potentially similar events, we selected small magnitude events ($1.0 \leq m_l \leq 2.5$) between 5- and 10-km depth in a small area (Figure 1). This magnitude range contains 80% of the events that occurred in the volume investigated. To avoid unusable events, we used only events with more than 12 $P$ wave first arrival readings. We did not try to use any closeness criterion to select the set of data, location errors being possibly larger than the actual interevent distances. Finally, 1095 events fitting these simple magnitude and location criteria were collected. They cover the period from 1979 to 1982. The seismic crisis related to the eruption of January 1983 is not included in the initial set of data, and therefore no selected events belong to this crisis.

## Method

The cross-spectral method [*Jenkins and Watts*, 1968] is used to perform both multiplet selection and time delay computation.

### Multiplet Selection

We can first define a multiplet as a set, and a doublet as a pair of similar-appearing events. To characterize the degree of similarity of a pair of events, we use the modulus of the coherency spectrum (or coherency), which is the smoothed cross-spectrum normalized by the smoothed autospectra of each windowed seismogram. The smoothing function of the spectral densities is the Fourier transform of a Tukey window of order two. The most concise way to represent the similarity of the whole set of events with a minimum loss of information is to compute the coherency for each pair of events. With this aim, we compute a mean coherency, defined as the average of the coherency calculated on the first 1.28 s of the signals recorded on four stations, in the frequency band 4-12 Hz. The four stations chosen are close to the common epicenter. They recorded impulsive signals and operated during the whole period.

## Time Delay Computation and Multiplet Relative Relocation

A multiplet is relocated from the set of time delays computed for each doublet in it. Time delay between two similar signals corresponds to the abscissa of the maximum of their cross-correlation function. As the cross spectrum is the Fourier transform of the cross-correlation function, time delay is proportionnal to the slope of the cross-spectrum phase. For one doublet, computation of time delays between two windows of the signals recorded at each station is therefore carried out from the weighted linear adjustment of the phase of the cross spectrum [*Poupinet et al.*, 1984; *Fréchet*, 1985]. Each window of 1.28 s is first centered on each $P$ time calculated using a common hypocenter, then aligned to the closest sample. The weight used is proportional to the reciprocal of the variance of the cross-spectrum phase:

$$w_k^2 = C_k^2 / (1 - C_k^2) \qquad 90\% \leq C_k < 100\%$$
$$w_k^2 = 0. \qquad\qquad\qquad C_k < 90\%$$

(1)

where $C_k$ is the coherency for the $k$th frequency sample. Time delays are retained if the mean coherency in the frequency band 4-12 Hz is greater than 90%.

For very similar signals, this procedure provides more accurate estimates of time delay than the direct calculation using a cross correlation function. Time delay is directly calculated from the linear fit of the cross-spectrum phase, which avoids any interpolation of the cross-correlation to obtain its actual maximum. Coherency is used to weight the fit and allows only high signal to noise frequency samples to be taken into account.

Errors in time delay computation can arise from coherency drops and from differences in the instrumental delays introduced during the digitization process carried out for each event constituting the doublet. Variations in the coherency $C$ lead to an uncertainty in the time delay that reaches less than a few milliseconds for coherencies greater than 90%. Origins of instrumental delays introduced by a digitization system similar to the one we used have been carefully discussed by *Poupinet et al.* [1984]. Changes in tape speed, total instrumental response, digitization channel, and telephone line delay can occur. However, all stations used were digitized on the same tape, so that there is no need to correct for tape
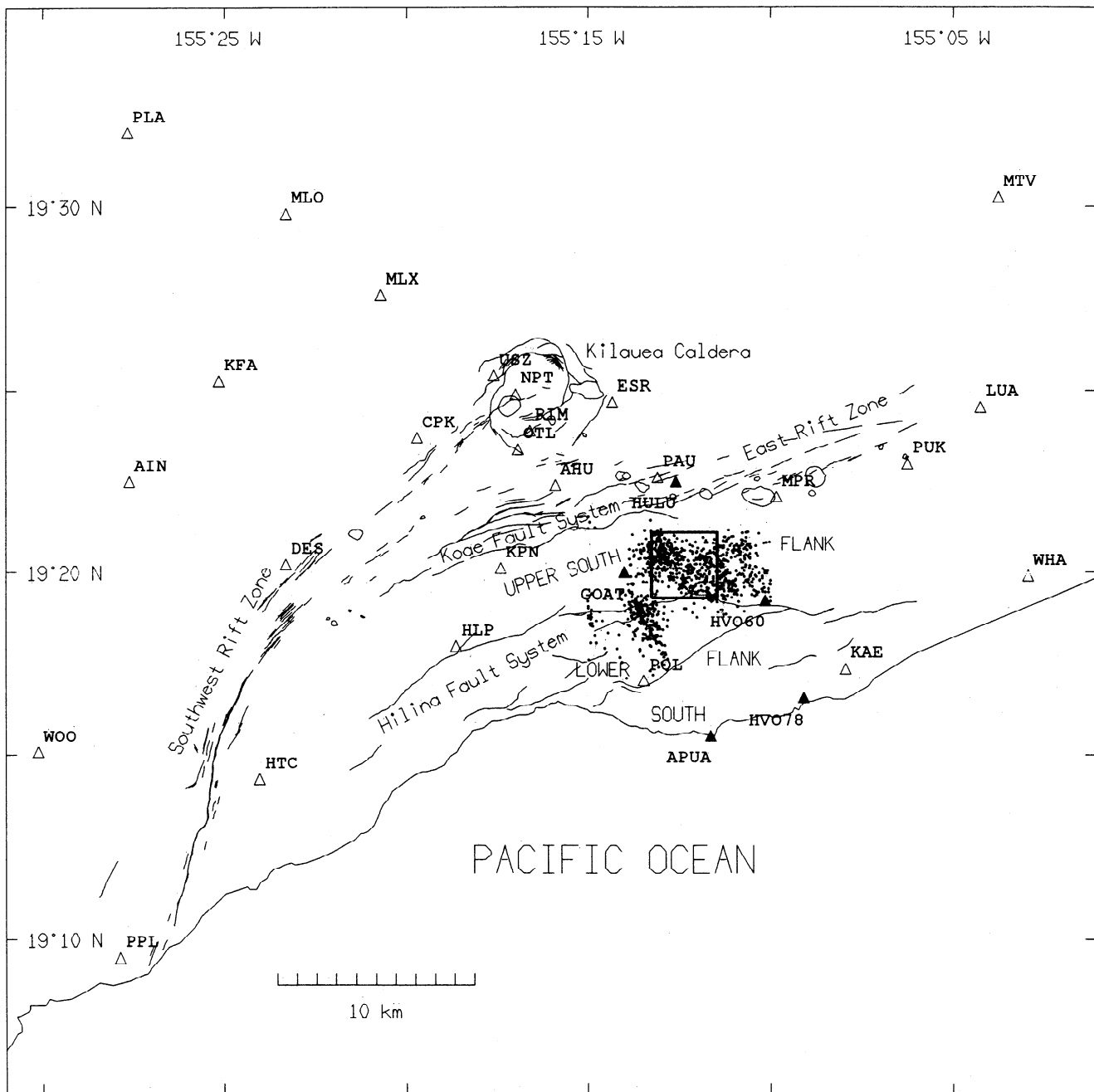
**Figure 1.** Map of Kilauea and adjacent part of Mauna Loa volcanoes, Hawaii, showing rift zones, fault systems, craters, and epicenters of microearthquakes from the initial selection (dots). Bold open square shows the limits of the map of the relocated events (Figure 3b). Initial set of data has been selected in a volume whose limits are 19°16'00" and 19°22'00" (latitude), 155°10'00" and 155°15'00" (longitude), 5- to 10-km depth. Locations of HVO seismic stations and geodetic benchmarks are indicated by open and solid triangles, respectively. HULU is the label for Huluhulu geodetic benchmark.

speed variations. In this study, our purpose is not to relocate some events with an accuracy of a few meters as performed by *Fréchet* [1985], but rather to relocate a large set of events having the largest possible spatial extent with a time precision of a few milliseconds. We will see if the use of a large set of stations, and the use of a weighting function which rejects aberrant time delays during the relocation process, will provide sufficiently accurate results.

To relocate one event of a doublet relative to the other, we will follow a method derived from that of *Fréchet* [1985]. Let us call the coordinates of one event relative to the other $x$, $y$, and $z$ (positive to the east, north, and down, respectively), $T$ the difference in origin times, and NSTA the number of stations recording the doublet. We can write the time delay between two events of a doublet recorded at the $k$th station situated at the azimuth $Az_k$ and the take-off angle $Ain_k$ from their common hypocenter

(estimated as the barycenter of both absolute locations) as

$$\Delta T_k = (\sin Az_k \sin Ain_k\, x + \cos Az_k \sin Ain_k\, y$$
$$+ \cos Ain_k\, z)\, /\, v + T, \quad (2)$$

where $v$ is the $P$ wave velocity at hypocentral depth.

In expressing the whole set of NSTA time delays as a function of $x$, $y$, $z$ and $T$ coordinates, we find a system of linear equations

$$\mathbf{Gm = d} \quad (3)$$

where $\mathbf{d}$ is the data vector (time delays) and, for a doublet, $\mathbf{G}$ is a NSTA x 4 matrix containing the partial derivatives of $\Delta T_k$ relative to the unknown vector $\mathbf{m} = (x, y, z, T)^T$.

For a multiplet including NEV events recorded by NSTA stations, (3) is a (sparse) system of NEV(NEV-1)NSTA/2 linear equations and 4(NEV-1) unknowns.

In the classical earthquake location methods, as in the *Fréchet* [1985] method of relative relocation, similar systems are solved using the Lanczos decomposition of $\mathbf{G}$. However, as the size of $\mathbf{G}$ increases as NEV³, this computation becomes very expensive for large multiplets (NEV > 50). First computations with the Lanczos method have shown that the system was generally well conditioned, with condition numbers ranging from 20 to 50.

In that case, there is an attractive way to reduce the size of our system; it consists of following the classical least squares approach and solving the (weighted) normal equations

$$\mathbf{G^T C_d^{-1} G m = G C_d^{-1} d} \quad (4)$$

to find

$$\mathbf{m = (G^T C_d^{-1} G)^{-1} G^T C_d^{-1} d} \quad (5)$$

where $\mathbf{C_d}$ is the data variance-covariance matrix.

As we can compute directly each element of the matrix $\mathbf{G^T C_d^{-1} G}$ by deriving the misfit function relative to $\mathbf{m}$, there is no need to store $\mathbf{G}$. $\mathbf{G^T C_d^{-1} G}$ is a symmetric positive definite matrix, and the solution $\mathbf{m}$ is found by performing (after an appropriate scaling) the Cholesky decomposition of $\mathbf{G^T C_d^{-1} G}$.

It is often useful to relocate $p$ new events relative to $n$ already relocated events. In that aim, the weighted normal equations can be written (subscripts refer to dimensions of the matrices)

$$((\mathbf{G^T C_d^{-1} G})_{4p,4p}(\mathbf{G^T C_d^{-1} G})_{4p,4(n-p)})(\mathbf{m}_{4p}\mathbf{m}_{4(n-p)})^T$$

$$= \mathbf{G^T C_d^{-1} d} \quad (6)$$

and the solution $\mathbf{m}$ for the $p$ new relative relocations becomes

$$\mathbf{m}_{4p} = (\mathbf{G^T C_d^{-1} G})^{-1}_{4p,4p}\, (\mathbf{G^T C_d^{-1} d}\, -$$

$$(\mathbf{G^T C_d^{-1} G})_{4p,4(n-p)}\mathbf{m}_{4(n-p)}) \quad (7)$$

Since each time delay is estimated with an error, each equation will be weighted to take this error into account. However, time delays are computed with two kinds of errors: coherency-dependent errors and possible errors due to different instrumental delays. The use of a weight merely inversely proportional to the error in the time delay, which we compute from the linear fit of cross-

spectrum phase, will therefore not be appropriate, since it corresponds only to a part of the error and strongly favors very coherent pairs of signals. To retain a maximum number of significant time delays and to reject those that are aberrant (but possibly coherent), we follow *Fréchet* [1985] and use the bi-square weighting proposed by *Mosteller and Tukey* [1979]:

$$W_k = \max\, (0,\, 1 - (R_k/(\alpha R_{med})^2)^2 \quad (8)$$

where $R_k = \Delta T_k - \Delta \tau_k$ is the residual on each time delay $\Delta T_k$, $\Delta \tau_k$ being the theoretical time delay computed for the $k$th station after relative relocation, and $R_{med}$ is the median of the set of absolute values of $R_k$.

This weight rejects observations that give residuals whose absolute value is $\alpha$ times greater than the median; $\alpha$ is usually chosen between 4 and 6.

The initial solution is obtained for unit weights. The inversion process is then iterated and the weight is modified at each step. The process stops when the rms reaches a minimum value or when the maximum iteration number is reached. Usual well-coherent multiplets require two or three iterations to be relocated.

The variance-covariance matrix of the model estimates is given by:

$$\mathbf{C_m = (G^T C_d^{-1} G)^{-1}} \quad (9)$$

However, errors computed as the square root of the diagonal elements of $\mathbf{C_m}$ are underestimated, since uncertainty in $\mathbf{G}$ is not taken into account in (9).

This method of relative relocation is much faster and less expensive in memory requirements than a singular value decomposition. It allows the use of time delays computed for the whole set of event pairs, even when these pairs are numerous. From that point of view, the method proposed is not a master event technique, as that used by *Fréchet* [1985], *Ito* [1985], *Scherbaum and Wendler* [1986], *Frémont and Malone* [1987] and *Deichmann and Garcia-Fernandez* [1992]. In a master event location, each event is relocated relative to only one event (the master event), no additional constraint being provided by the other events. The use of all possible pairs of events strongly increases the relocation accuracy, which is furthermore no longer dependent on the choice of a master event. Indeed, in the original master event technique, a good master event needs to be coherent with each event, that is, it should occupy a central position in a multiplet of small spatial extension. *Ito* [1985], *Scherbaum and Wendler* [1986] and *Frémont and Malone* [1987] already noticed that the relocation error increases with distance from the master event.

## Results

### Multiplet Selection

Coherencies have been computed for each possible pair of events. Results of the computation of coherencies (Figure 2) show that numerous pairs of events have a coherency greater than 90%. Figure 2 is a plot of the coherency computed for each possible pair of the initial set of 1095 events. It exhibits numerous highly coherent pairs (doublets), more or less confined along the main diagonal, which means that a significant part of the seismicity occurs during limited crises in time and space.
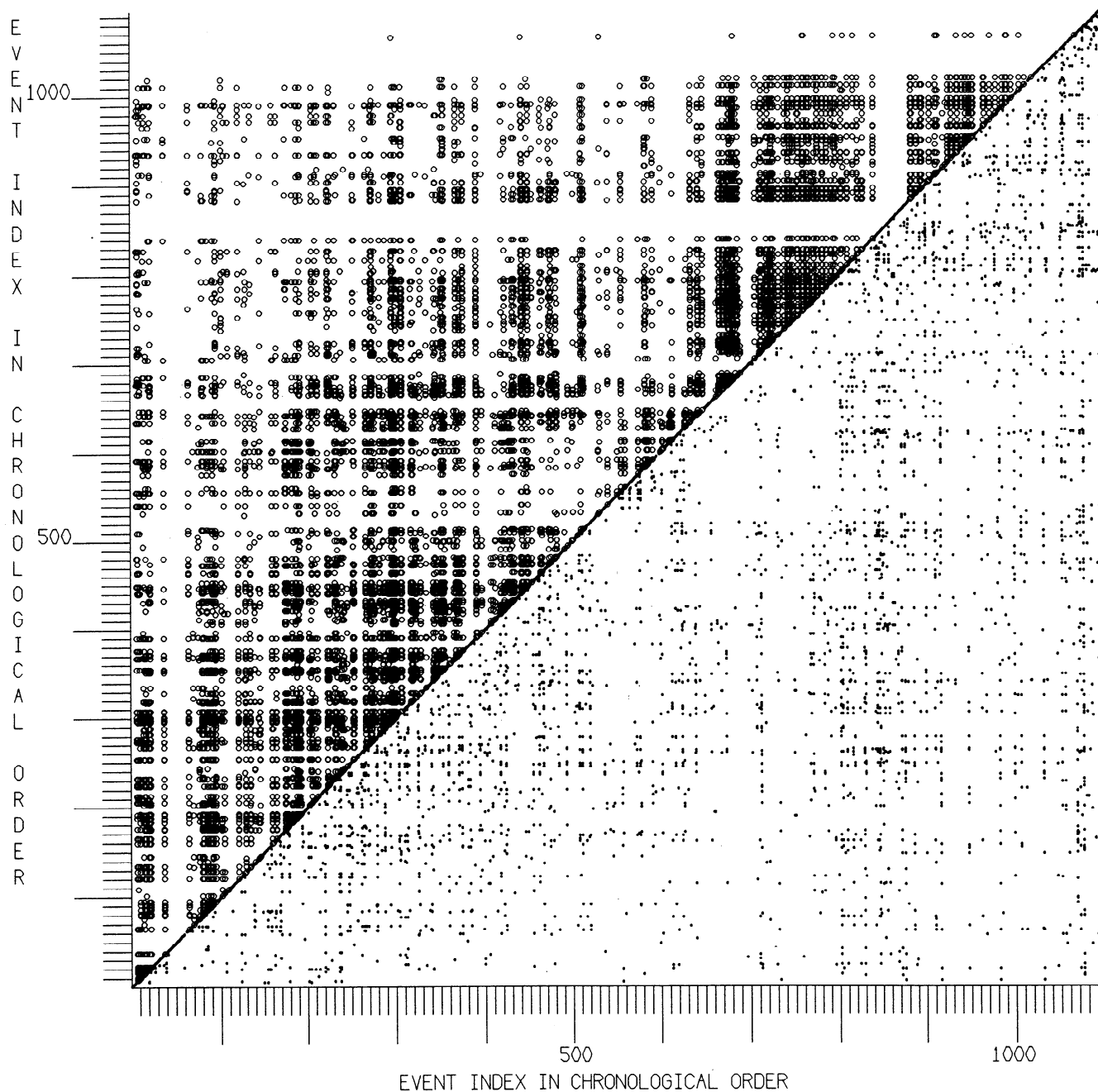
**Figure 2.** Plot of the coherency for all possible pairs of the initial selection (1095 events). (Top) Open circles: plot of the coherency for the relocated multiplet (252 events). (Bottom) Dots: plot of the coherency for the nonrelocated part of the initial selection (843 events). Each dot or open circle indicates a coherence greater than 90% for the corresponding pair of events. Each coordinate is the index of each event in the chronological list of earthquakes selected. Notice the high number of coherent pairs (doublets) in the initial selection, and the strong proportion of doublets from the inital selection finally relocated (top).

The matrix formed by the coherency computed for each possible pair is used to select similar events and group them into multiplets. In this study, we define a multiplet as a set in which each element has at least 90% coherency with at least 30 other events of the multiplet. This definition is controlled by two parameters: the coherency threshold above which a pair is accepted as a doublet, and the minimum number of events (neighbors) which can be paired as doublets with each element of the

multiplet. The coherency threshold guarantees the accuracy of the time delay computation, and the minimum number of doublets used to relocate each event of the multiplet has been introduced to limit relocation errors.

To illustrate the effect of this minimum number of doublets used to relocate each event, let us define a sensu lato multiplet and a sensu stricto multiplet. A sensu lato multiplet is a set in which each element has to be

coherent with at least one other element of the multiplet. In that case our data provide a multiplet formed by a gigantic chain of doublets composed of 837 events. However, most members of the so-defined multiplet will be a doublet with only one other element of the multiplet, and therefore cannot be accurately relocated, because of error propagation. Alternatively, we can define a sensu stricto multiplet as a set in which each element has to be coherent with all other elements of the multiplet. With our data, this sensu stricto definition finds multiplets comprising a few events, and therefore having a small extent.

Using a minimum number of 30 doublets per event in a multiplet, we found a multiplet containing 252 events (Figure 2, top). It takes into account most similar events of the initial set of 1095 events. Figure 2 (bottom) shows that there is no other major multiplet in our data.

## Multiplet Relocation

Our aim is to relocate as accurately as possible the multiplet having the largest spatial extent. However, we cannot relocate accurately at one time those events that are not similar from one end of the multiplet to the other, especially if the spatial extent of the multiplet is large. Indeed, the number of event pairs for which the mean coherency is greater than 90% strongly drops when the distance between them increases. Further, above an interevent distance of about 500 m (less than 10% of the distance to the nearest station), the assumption we made that the time delay is due only to the difference in hypocenter locations is violated. Finally, azimuths and take-off angles used in the computation, calculated from

the common barycenter, become erroneous for the closest stations when the spatial extent increases. As a result, the relocation of a multiplet is conceived as an iterative process. An initial multiplet, containing a high number of very coherent doublets, is first relocated. In our study, this initial multiplet comprises 80 events having 95% coherency with more than 30 of its events. The relocation process continues by relocating individual events for which coherency with a minimum number of events (30 in this study) of the current set reaches a minimum value (90%). At each step the current set of already relocated events is updated. This process ensures that each new event will be relocated relative to its closest neighbors. Lower values of both coherency and number of neighbors used in the relocation lead to a greater number of relocated events but also more location errors.

The 252 events of the multiplet selected have been relocated with an average relative error of about 50 m horizontally and 75 m vertically revealed by Monte-Carlo simulations. Series of such simulations show that the error in location is proportional to the error in delay, azimuth, and take-off angle, and inversely proportional to the square root of the number of events. Due to the relatively poor take-off angle distribution, horizontal as well as vertical errors are strongly dependent on the error in take-off angle.

The 252 relocated events represent a large part of the events which can be paired as doublets in the initial selection (Figure 2) and define a small subhorizontal planar volume (Figure 3a). Changing the velocity or introducing an isotropic velocity gradient in the relocated volume induces a linear (homothetic) deformation of the
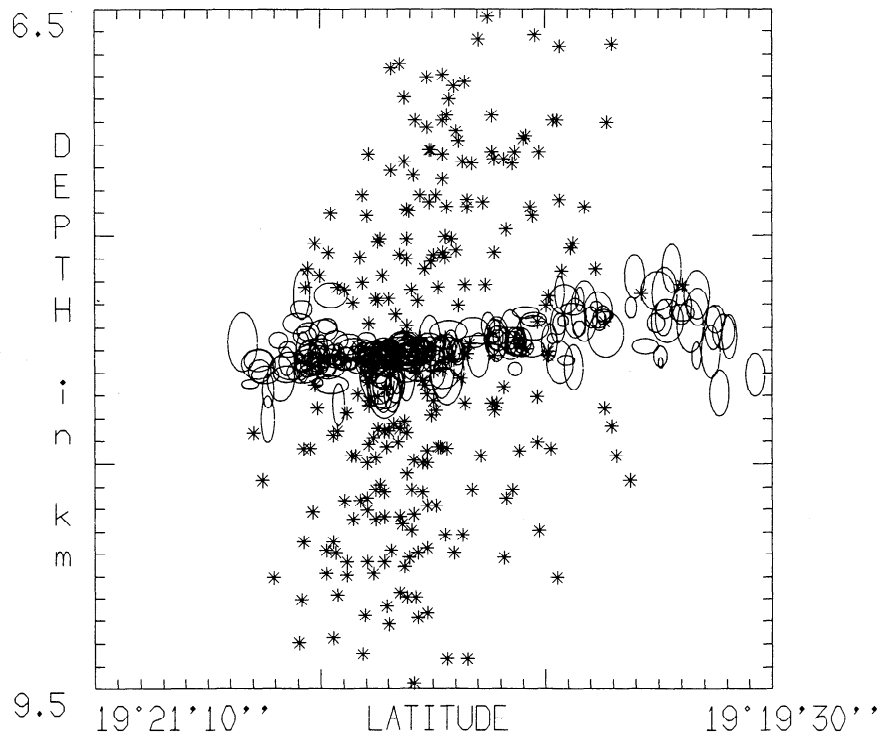


**Figure 3a**. Projection of the relocated cluster on a N-S vertical plane showing absolute locations (stars) and relative relocations with their 90% confidence ellipses (open ellipses). Relative relocations and absolute locations are assumed to have the same center of gravity.
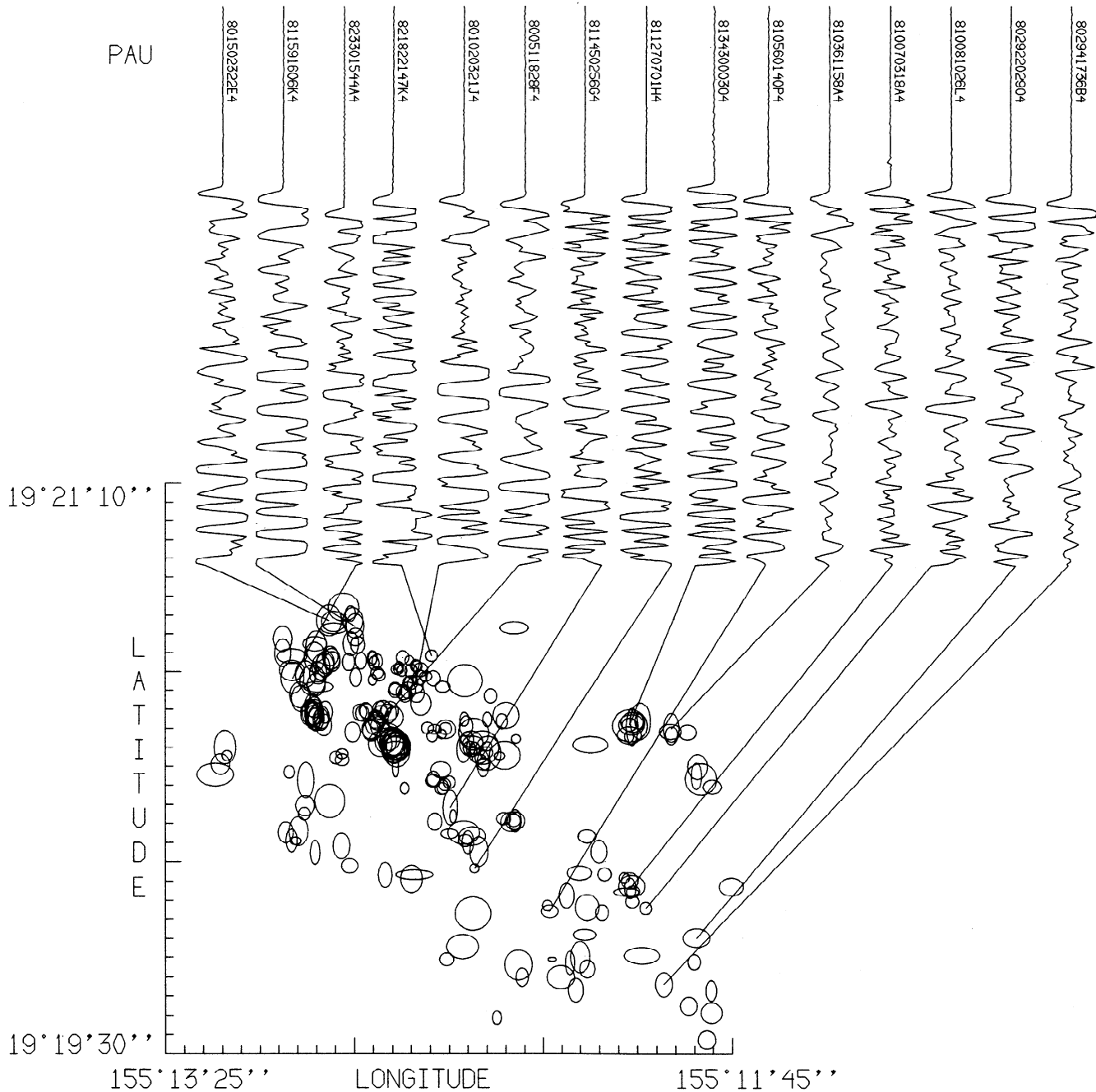
**Figure 3b.** Map of the relocated multiplet. Seismograms (2.00 s) recorded at PAU seismic station are plotted for the sample of events used to construct the focal mechanism.

planar cloud of relocations but does not modify its direction and dip. Since relative relocations show that actual hypocenters have about the same depth, we remove random errors and improve the estimate of the multiplet absolute depth by averaging the absolute depths provided by HVO summary files for each event of the multiplet. We obtain an absolute depth of about 8 km for the multiplet. Such averaging cannot eliminate a possible systematic bias due to the velocity model used for the absolute locations.

## Discussion

The absolute catalog locations of our multiplet form a 3-km-high cloud at an average absolute depth of 8 km.

After relocation, they lie in a thin band about 100-200 m thick (Figure 3a). This thickness is of the order of the computed vertical error on the relative relocations (75 m), and is therefore close to the resolution of the method with the data collected. This small thickness, compared to the vertical error and to the horizontal extent of the multiplet (about 4 km²), and the perfect similarity of the focal mechanisms in this small planar volume, lead us to the conclusion that these events occurred on the same fault plane or on a very thin shear zone. Thus most of the apparent vertical scatter of the absolute locations we used is due, as *Crosson and Endo* [1982] stated, to location errors. It therefore solves locally the apparent contradiction between the cylindrical distribution of the

seismicity in the northernmost part of the south flank, and the existence of a subhorizontal fault plane, inferred by numerous authors [e.g. *Swanson et al.*, 1976; *Ando*, 1979]. Our results thus confirm the suggestion of *Crosson and Endo* [1982] that a significant part of the seismicity could be confined to a thin layer between 5- and 10-km depth. We do not conclude that all south flank earthquakes reduce to a single plane, since the relocated multiplet represents only a part of the seismicity. However, no other major multiplet is present in our data (Figure 2, bottom).

To infer average parameters characterizing the spatial distribution of the relocated hypocenters, we have chosen to fit them by a simple planar model, although a careful examination of Figure 3a can lead to many alternative and more complex models, including multiple planes or flat-and-ramp models. Such a planar least squares fit shows that the relocated hypocenters determine an average N90°+-30° striking, 6°+-4°N dipping plane. The 90% confidence intervals are indicated for the parameters of this model. Other more detailed models, as flat-and-ramp models, lead to determine up to 12°+-3°N dip ramps.

The average N90° striking, 6°N dipping plane is compatible with the subhorizontal fault plane solution inferred from the focal mechanism of the multiplet (Figure 4). To construct this focal mechanism, azimuths and take-off angles have been computed using the linear gradient velocity model of *Klein* [1981], the depth of each event being forced to be 8 km, the average absolute depth of the multiplet events. We used a set of events providing a correct spatial sampling of the multiplet. Individual focal mechanisms constructed for each event give the same focal solutions; all stations show the same polarities in all focal mechanisms, except MPR, which straddles a nodal plane (Figure 4). We therefore decided to plot each polarity read for MPR for each event of the set on the same focal mechanism. MPR and the farthest northwestern stations permit constraint of the dip of both vertical and horizontal planes. Station HLP always indicates dilation. Although there remains uncertainty in the direction of the horizontal fault plane, its northwestward 5° dip corresponds very closely to the dip we infer from multiplet relocation. Our fault plane solution is very close to that presented in the northwesternmost focal spheres plotted in Figures 6 and 7 of *Bryan*'s [1992] study of the June 1989 $M_s$= 6.1 Kilauea south flank earthquake. *Chen and Nabelek* [1990] also found a similar focal solution for the later mainshock from inversion of teleseismic *P* and *SH* waves. Notice that the statistical significance of our relative relocations and focal mechanism is comparable to that of a major earthquake, as the relocated area covers about 4 km². Relocation allows us to have a clear picture of the local microseismicity and removes the ambiguity between nodal planes.

The fault plane determined by *Ando* [1979] for the Kalapana earthquake of November 1975 ($M_s$ = 7.2), from surface wave and tsunami analysis, was a N70°E striking, 20°SSE dipping normal fault. More recently, using additional first-motion polarities of *P* waves constraining the vertical auxiliary plane, *Kovach and Hill* [1987] determined a strictly horizontal N53°E fault plane solution for the same event. The plane we found, which

generates most of the local microseismicity, is not a southeastward-dipping plane, as could be expected from *Ando*'s [1979] study. The average northward dip of our multiplet plane is about three times greater than northward dips previously inferred (*Zucca and Hill* [1980]; *Zucca et al.* [1982]; *Crosson and Endo* [1982]). *Thurber and Gripp* [1988] carried out flexure calculations to determine reliable estimates of the average dip due to the load of the volcano on the oceanic crust. They found, below the south flank, a northwestward dip of about 1°-2°. There is less than 5% probability for the plane we found to have a northward dip lower than 2°. Major interfaces, such as the top of the oceanic crust or the Moho discontinuity, have very monotonous slopes below the island of Hawaii. A difference of about 5° along a 50-km-long distance would lead to an error of about 4 km on the depth of these major interfaces, and could not be unnoticed by *Zucca and Hill* [1980] and *Zucca et al.* [1982], nor in the calculations of *Thurber and Gripp* [1988]. The plane we found is therefore too steep to be confused with the regional flexure of the basal layer. This relatively steep slip plane below the upper south flank is much more active seismically than other areas, especially the lower south flank. It probably represents a local irregularity rather than the overall geometry of the basal slip plane, where slip is sometimes aseismic and could occur on a more accordant subhorizontal decollement plane. Consequently, we hypothesize that the basal slip plane has different dips below the upper and lower south flank (Figure 5). In the following paragraphs, we will check this hypothesis using semiqualitative arguments. A complete discussion would require numerical simulations of ground deformations, which are beyond the scope of this work.

The geometry of the deep slip plane affects observable surface deformations. Consequently, we compared our result with available geodetic measurements (Figure 5): long-term surface deformation of the south flank [*Swanson et al.*, 1976], coseismic deformation during the 1975 Kalapana earthquake [*Lipman et al.*, 1985], and short-term features of the ground deformation [*Swanson et al.*, 1976; *Delaney et al.*, 1992]. Many of these geodetic observations are compatible with the existence of a northward-dipping plane.

The northward dip of the plane forces the displacement of the south flank to have an upward component. Uplift, with a maximum immediately south of Kalanokuaiki Pali at the south boundary of the Koae fault system, has been well documented [*Fiske and Koyanagi*, 1968; *Swanson et al.*, 1976]. It is generally interpreted as the result of magma intrusions into dykes in the rift zones and consequent compression of the south flank [*Swanson et al.*, 1976]. It has been modeled by *Dvorak et al.* [1994] to result from both compression and slip on a basal plane. Our result is compatible with theirs. Uplift of the upper south flank can be due to southward displacement and consequent compression on a northward-dipping slip plane.

Coseismic deformations recorded during the Kalapana earthquake show that the upper south flank behaves as an anomalous zone relative to the rest of the south flank. Indeed, maps and cross sections of the vertical displacements of the south flank after the Kalapana
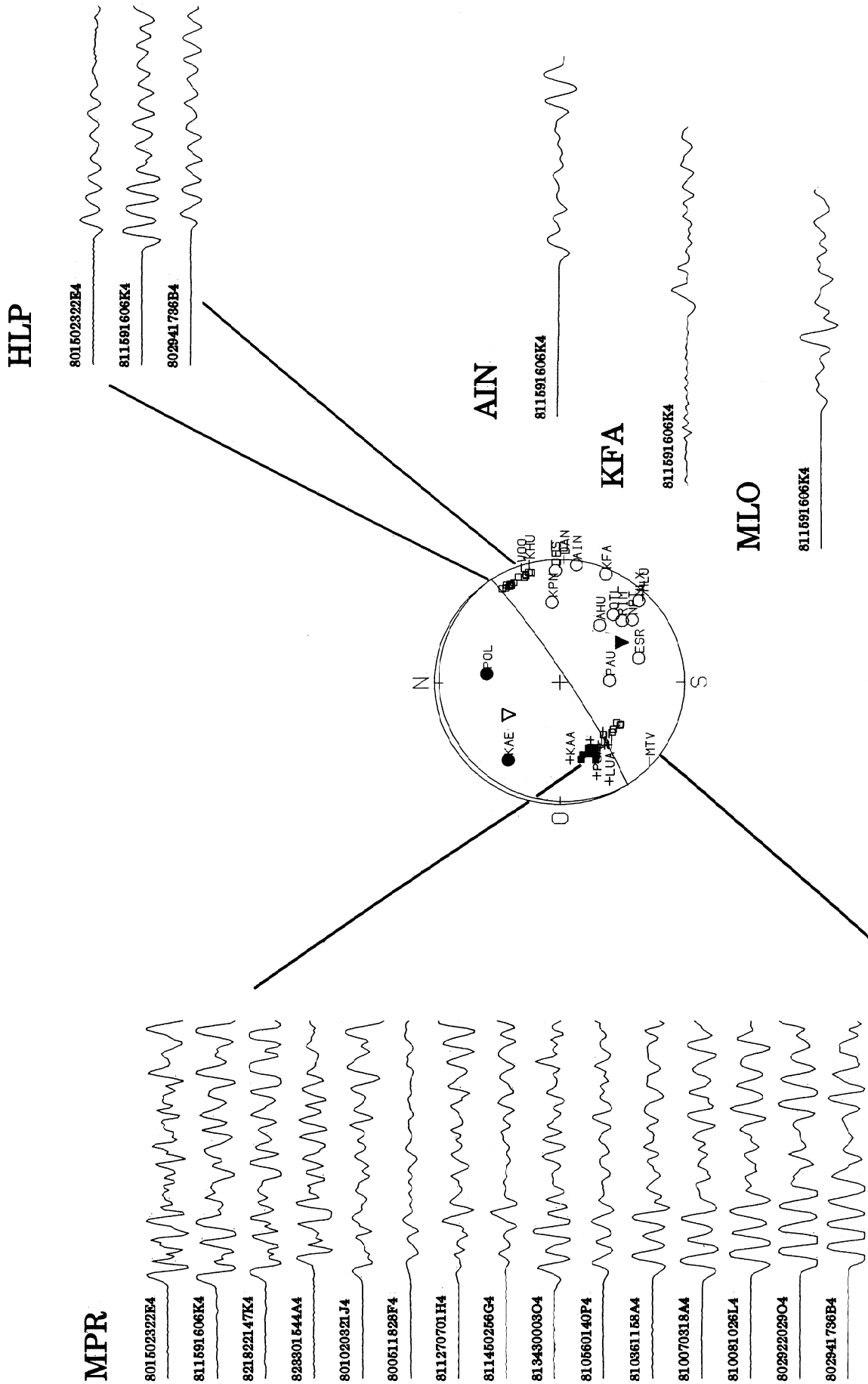
**Figure 4.** Focal mechanism of the relocated multiplet. Seismograms (2.00 s) recorded at MPR seismic station are plotted for the sample of events used in Figure 3b. MPR and HLP polarities are plotted for each event of the sample. For the other stations, polarities do not change, and azimuths and take-off angles do not vary significantly. Seismograms (2.00 s) recorded at HLP seismic station are plotted for the more significant events of the sample. For the same duration, seismograms recorded at AIN, KFA, MLO seismic stations are plotted for the more energetic event.
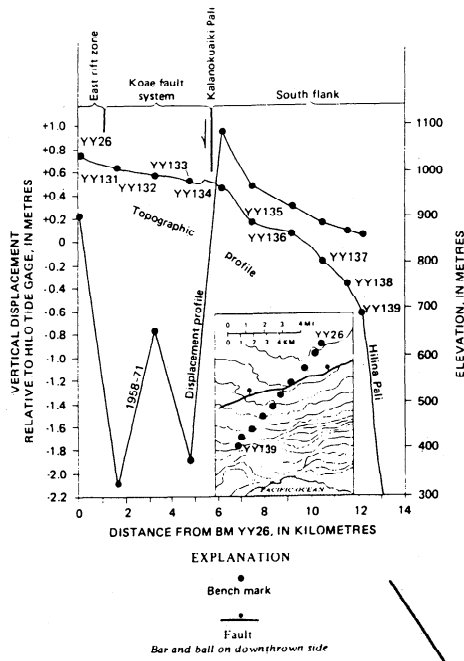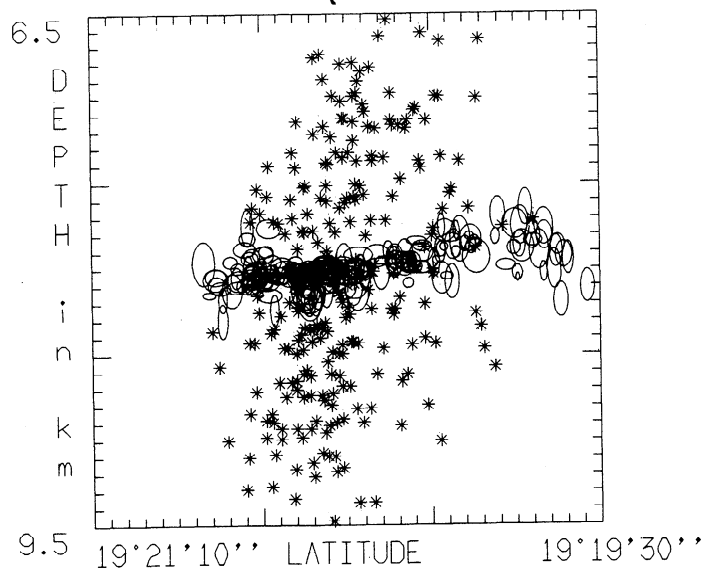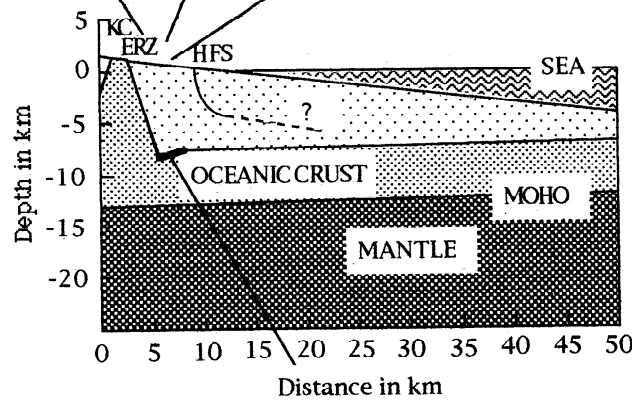
From Swanson et al. (1976)
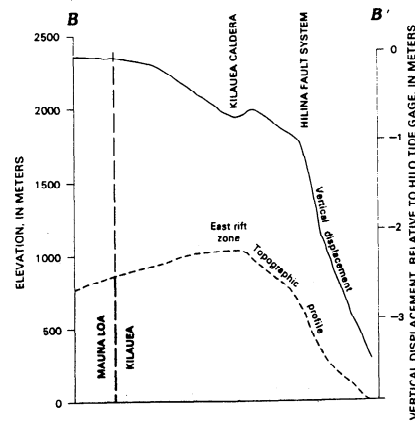
From Lipman et al. (1985)
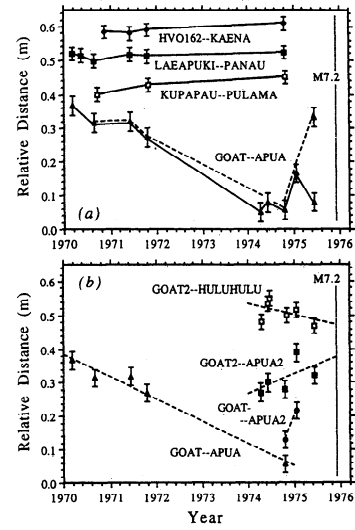
From Delaney et al. (1992)

**Figure 5**. Schematic cross section showing the main features of Kilauea's south flank. KC, Kilauea caldera; ERZ, east rift zone; HFS, Hilina fault system. Crustal structure is reprinted from *Zucca and Hill* [1980].

earthquake, presented by *Lipman et al*. [1985], indicate a general downward displacement with minimum subsidence near the north margin of the upper south flank (Figure 5). The horizontal component of the southward displacements of the south flank (up to 8 m) increases continuously from north to south and shows horizontal extension. Strikingly, the vertical (downward) component of the displacements is far smaller in the upper south flank (less than 0.7 m) than in either the lower south flank (up to 3.5 m) or Kilauea caldera (up to 1.4 m). The southward increase in the extension of the south flank produces a very irregular vertical subsidence, with a relatively stable band [*Lipman et al.*, 1985] situated just above the northward-dipping plane we found. We agree with *Thurber and Gripp*'s [1988] idea that the configuration of the decollement controls the growth of Kilauea's rift zones. They noticed that the oceanic crust is more deeply depressed and steeply dipping below the southwest rift zone than below the east rift zone. They proposed that the geometry of the decollement layer is responsible for the different rates of eruptive activity of the two rift zones. Further interpretations of the coseismic displacement map of *Lipman et al*. [1985] will have to take into account the hypothesis of a relatively steep northward-dipping slip plane below the upper south flank.

Short-term geodetic data also show that the upper (northern) and lower (southern) south flank have different behavior. *Wyss et al*. [1981] used short-term geodetic data to analyze the slip of different parts of the south flank. They identified the northwestern upper part of the south flank near the earthquake cluster we studied as a major asperity that ruptured during the 1975 Kalapana earthquake. More recently, *Delaney et al*. [1992] corrected the geodetic data used by Wyss et al. (1981) and reassessed their conclusions. In Figure 2b of *Delaney et al*. [1992], carefully processed geodetic data show that the Goat2 - Huluhulu geodetic line (Figure 1), directed north from Goat benchmark, continued to record strain accumulation during 1974-1975 (Figure 5), whereas Goat2 - Apua2, directed south from Goat (Figure 1) began to have strain release. During 1974-1975, Huluhulu moved southward under the effect of magma intrusion, whereas the upper part of the south flank near Goat remained locked. During the same period, the lower part experienced dilation and moved seaward with the neighboring easternmost parts. A steeper dip of the basal layer below the upper south flank could explain the strain accumulation north of Goat and the strain release south of Goat during 1974-1975. The same geometry of the decollement zone (Figure 5) could be responsible for some important features (long-term uplift, Kalapana coseismic deformations, short-term ground deformations) of the response of the south flank under forceful intrusion of magma into the east rift zone.

Figure 2a of *Delaney et al*. [1992] displays, in the horizontal displacement of the south flank measured along the line Goat - Apua, a striking feature already observed by *Swanson et al*. [1976] along the line HVO60 - HVO78 (Figure 1). Both sets of measurements show a time series of high-rate contractions alternating with low-rate extensions. This strongly suggests stick-slip in the south flank. *Swanson et al*. [1976] correlated extension

episodes with $m_l \geq 3.5$ events of the south flank. Figure 2 of *Delaney et al*. [1992] supported the idea that low-rate extension episodes recorded south of Goat are the response of the western lower part of the south flank to accommodate the seaward displacement of the eastern part, whereas farther north, the asperity is locked. Although of small amplitude, such repeated extension episodes could have been sufficient to initiate the normal faults in the Hilina fault system. However, these extension episodes do not balance the overall contraction of the south flank, and most of the strain accumulated in the northwestern region is probably released during major earthquakes [*Wyss et al*., 1981; *Lipman et al*., 1985]. *Lipman et al*. [1985] have shown that much of the Hilina fault system was activated during the 1975 Kalapana earthquake and accounts for the largest surface deformations. Those have been recorded in the lower south flank, the western asperity being situated at the top of the zone of maximum coseismic displacement gradient. The Goat region accumulated more strain than the easternmost regions before the 1975 Kalapana earthquake, as indicated by Figure 2 of *Delaney et al*. [1992], and released it coseismically. Additionally, the fact that coseismic deformations are stronger in the Hilina fault system than in the Goat region supports the conclusion that the rupture of the Goat asperity triggered the movement of the Hilina fault system, locally amplifying deformations. The south flank of Kilauea appears to be an unstable system, where stresses are accumulated in the upper south flank, whereas the lower south flank experiences aseismic deformation and can slip more easily than the upper part along a near-horizontal decollement plane (Figure 5). This model is consistent with the idea of *Bryan* [1992], who suggested that relatively small-magnitude events of the (upper) south flank could trigger large-scale energy release and surface deformation.

## Conclusion

A large set of seismic events was selected from the upper south flank of Kilauea Volcano, Hawaii. Systematic selection of similar events was carried out by computing the coherency for each event pair of the set. The quality of the data and the similarity of the signals are sufficient to determine accurate time delays. A simple and efficient method has been developed which allowed relative relocation of more than 250 events with an average precision of about 50 m horizontally and 75 m vertically at about 8 +- 1.5 km depth. Relocated hypocenters cover an area of about 4 km$^2$ and define a 6° +- 4° northward-dipping plane at about 8-km depth. This plane is responsible for a large part of the local seismicity and can be considered as a major feature of the upper south flank. Other deep fault planes of less extent having different dips and depths, or experiencing aseismic slip, cannot be discarded.

The plane we infer from multiplet relocation is clearly steeper than the regional flexure of the oceanic crust under the load of the volcanic pile. It could be a local irregularity of the decollement layer below the upper south flank. Seismicity and surface deformations exhibit strong differences between the upper and lower south

flank that could be related to the geometry of this deep fault plane.

Multiplet relocation provides accurate basic information at depth that can be suitable to further work, including numerical simulations, necessary to better understand results of surface deformation measurements. Such a method of relative relocation of multiplets could be used in other highly seismic areas to provide accurate information on deep fault-plane geometry, seismicity patterns, and earthquake generation processes.

# References

Ando, M., The Hawaii earthquake of November 29, 1975: Low dip angle faulting due to forceful injection of magma, *J. Geophys. Res., 84*, 7616-7626, 1979.

Arnadottir, T., P. Segall, and P. Delaney, A fault model for the 1989 Kilauea south flank earthquake from leveling and seismic data, *Geophys. Res. Lett., 18*, 2217-2220, 1991.

Bryan, C. J., A possible triggering mechanism for large Hawaiian earthquakes derived from analysis of the June 1989 Kilauea south flank sequence, *Bull. Seismol. Soc. Am., 82*, 2368-2390, 1992.

Bryan, C. J., and C. E. Johnson, Block tectonics of the island of Hawaii from a focal mechanism analysis of basal slip, *Bull. Seismol. Soc. Am., 81*, 491-507, 1991.

Chen, W. P., and J. Nabelek, Source parameters of the June 26, 1989 Hawaiian earthquake, *Eos Trans. AGU 71*, 562, 1990.

Crosson, R. S., and E. T. Endo, Focal mechanisms of earthquakes related to the 29 November 1975 Kalapana, Hawaii, earthquake: The effect of structure models, *Bull. Seismol. Soc. Am., 71*, 713-729, 1981.

Crosson, R. S., and E. T. Endo, Focal mechanisms and locations of earthquakes in the vicinity of the 1975 Kalapana earthquake aftershock zone 1970-1979: Implications for tectonics of the south flank of Kilauea volcano, island of Hawaii, *Tectonics, 1*, 495-542, 1982.

Deichmann, N. and M. Garcia-Fernandez, Rupture geometry from high-precision relative hypocentre locations of microearthquake clusters, *Geophys. J. Int., 110*, 501-517, 1992.

Delaney, P. T., Wyss, M., Lipman, P. W. and A. T. Okamura, Comment on "Precursors to the Kalapana M = 7.2 earthquake" by Max Wyss, F.W. Klein, and Arch C. Johnston, *J. Geophys. Res., 97*, 4839-4841, 1992.

Dvorak, J. J., Klein, F. W., and D. W. Swanson, Relaxation of the south flank after the 7.2 magnitude Kalapana earthquake, Kilauea volcano, Hawaii, *J. Geophys. Res.*, in press, 1994.

Eissler, H. K., and H. Kanamori, A single-force model for the 1975 Kalapana, Hawaii, earthquake, *J. Geophys. Res., 92*, 4827-4836, 1987.

Fiske, R. S., and R. Y. Koyanagi, The December 1965 eruption of Kilauea Volcano, Hawaii, *U.S. Geol. Surv. Prof. Pap., 607*, 21p., 1968.

Fréchet, J., *Sismogenèse et doublets sismiques*, Thèse d'Etat, 207 pp., Univ. Sci. Technol. Médic., Grenoble, 1985.

Frémont, M.-J., and S. D. Malone, High precision relative locations of earthquakes at Mount St. Helens, Washington, *J. Geophys. Res., 92*, 10,223-10,236, 1987.

Ito, A., High resolution relative hypocenters of similar earthquakes by cross-spectral analysis method, *J. Phys. Earth, 33*, 279-294, 1985.

Jenkins, G. M., and D. G. Watts, *Spectral Analysis and Its Applications,* Holden-Day, Oakland, Calif., 1968.

Klein, F. W., A linear gradient crustal model for south Hawaii, *Bull. Seismol. Soc. Am., 71*, 1503-1510, 1981.

Klein, F. W., R. Y. Koyanagi, J. S. Nakata, and W. R. Tanigawa, The seismicity of Kilauea's magma system, Volcanism in Hawaii, 2, *U.S. Geol. Surv. Prof. Pap., 1350*, 1019-1186, 1987.

Kovach, R. L., and D. P. Hill, The 1975 Kalapana earthquake revisited, paper presented at Hawaii Symposium on How Volcanoes Work, Hawaiian Volcano Obs., Hilo, Hawaii, 1987.

Lipman, P. W., J. P. Lockwood, R. T. Okamura, D. A. Swanson, and K. M. Yamashita, Ground deformation associated with the 1975 magnitude-7.2 earthquake and resulting changes in activity of Kilauea volcano, Hawaii, *U. S. Geol. Surv. Prof. Pap., 1276*, 45 pp., 1985.

Mosteller, F. and J. W. Tukey, *Data Analysis and Regression,* Addison-Wesley, Reading, Mass., 1979.

Poupinet, G., W. L. Ellsworth, and J. Fréchet, Monitoring velocity variations in the crust using earthquake doublets: An application to the Calaveras fault, California, *J. Geophys. Res., 89*, 5719-5731, 1984.

Scherbaum, F., and J. Wendler, Cross spectral analysis of Swabian Jura (SW Germany) three-component microearthquake recordings, *J. Geophys., 60*, 157-166, 1986.

Swanson, D. A., W. A. Duffield, and R. S. Fiske, Displacement of the south flank of Kilauea volcano: The result of forceful intrusion of magma into the rift zones, *U.S. Geol. Surv. Prof. Pap., 963*, 1-39, 1976.

Thurber, C. H., and A. E. Gripp, Flexure and seismicity beneath the south flank of Kilauea volcano and tectonic implications, *J. Geophys. Res., 93*, 4213-4248, 1988.

Wyss, M., and R. L. Kovach, Comment on "A single-force model for the 1975 Kalapana, Hawaii, earthquake" by Holly K. Eissler and Hiroo Kanamori, *J. Geophys. Res., 93*, 8078-8082, 1988.

Wyss, M., F. W. Klein, and A. C. Johnston, Precursors to the Kalapana M=7.2 earthquake, *J. Geophys. Res., 86*, 3881-3900, 1981.

Zucca, J. J., and D. P. Hill, Crustal structure of the southeast flank of Kilauea volcano, Hawaii, from seismic refraction measurements, *Bull. Seismol. Soc. Am., 70*, 1149-1159, 1980.

Zucca, J. J., D. P. Hill, and R. L. Kovach, Crustal structure of Mauna Loa volcano, Hawaii, from seismic refraction and gravity data, *Bull. Seismol. Soc. Am., 72*, 1535-1550, 1982.

J. Fréchet, Laboratoire de Géophysique Interne et Tectonophysique, Observatoire de Grenoble, B.P. 53X, 38041 Grenoble, France. (e-mail: frechet (at) lgit.observ-gr.fr)

J.-L. Got, Université de Savoie, 73376 Le Bourget-du-Lac, France. (e-mail: got (at) univ-savoie.fr)

F. W. Klein, U.S. Geological Survey, 345 Middlefield Road, Menlo Park, CA 94025. (e-mail: klein (at) puna.wr.usgs.gov)